ELSEVIER

Infrared Physics & Technology 37 (1996) 733–739

INFRARED PHYSICS & TECHNOLOGY

Superradiance and Raman scattering in three-level molecular system

A.V. Andreev [a,*], S.L. Sheetlin [b]

[a] *Physics Department, M.V. Lomonosov Moscow State University, Moscow 119899, Russia*

[b] *Department of Applied Mathematics, and Cybernetics, M.V. Lomonosov Moscow State University, Moscow 119899, Russia*

Received 18 December 1995

Abstract

A model is presented for the dynamics of superradiance, coherent and stimulated Raman scattering from an optically pumped three-level system. The evolution of the pumping and two counterpropagating waves in the adjacent transition are taken into account. The results of computer simulation show that by specifying the pumping pulse area, and active medium length and pressure we can control the parameters of the pulses in the adjacent transition. The possibilities of observing coherent Raman scattering dynamics, which are significantly different from that for stimulated Raman scattering, are shown. The results of simulation show that for the ultrashort pumping pulse the superradiative emission in the backward direction is formed within the coherence length near the entrance plane of the active medium.

1. Introduction

Recently detailed experimental researches on the superradiative emission of radiation with the wavelength of 100–500 μm by different molecular gases under optical pumping by CO_2-laser have been carried out [1–4]. These experiments have shown that the superradiance (SR) and stimulated Raman scattering (SRS) are very effective methods of nanosecond pulse generation in the far-infrared region (FIR) where the conventional methods can not be used for a number of reasons. First, the lack of the electro-optic materials in the FIR region does not allow one to construct the schemes of mode-locking or Q-switching. Second, the molecular gases, which are the most significant class of the active media in the FIR region, are low-pressure gases. Therefore, they are narrow band amplification systems. SR or SRS pulse parameters depend on the intensity, temporal width and detuning of the pumping pulse, as well as on the gas pressure. By varying these parameters we can control the parameters of SR and SRS pulses.

In this paper, we develop the mathematical algorithms which allow us to model adequately the process of SR and SRS emission in rotational transitions of the molecular gases under optical pumping by CO_2-laser. The calculated results and analysis for the effects of coherent pumping dynamics and propagation effects on SR and SRS emission are presented and discussed. We show how characteristics of the SR and SRS can be controlled by specifying certain characteristics of the pumping pulse. The possibilities of observing the coherent Raman scattering (CRS), which is characterized by a number of specific features distinguishing it from the regime of SRS, are shown.

* Corresponding author.

1350-4495/96/$15.00
PII S1350-4495(96)00015-1

2. Main equations

Experimental research [1] has shown that usually only one rotational transition in the upper excited vibrational state is involved into the SR or SRS emission. The cascade transitions in the excited or ground vibrational states were not observed. Therefore, we can use the three-level model to describe the interaction of molecules with the pumping and SR or SRS pulses. The sub-branches, which differ in the value of the projection of the angular momentum along the molecular axis, can contribute to the absorption or emission depending on the characteristics of the pumping pulses. However, because these transitions do not interfere with each other we can consider the active medium in this case as a mixture of the different three-level molecules.

The equations for slowly-varying amplitudes of electromagnetic waves $a_{n\alpha}$, polarizations $p_{n\alpha}$ and population densities n_k are

$$\frac{\partial n_3}{\partial t} = -\sum_n \sum_\alpha (p^*_{n\alpha} a_{n\alpha} + p_{n\alpha} a^*_{n\alpha}),$$

$$\frac{\partial n_2}{\partial t} = -\gamma_2 n_2 + \sum_\alpha ((p^*_{2\alpha} a_{2\alpha} + p_{2\alpha} a^*_{2\alpha}) - (q_\alpha b^*_\alpha + q^*_\alpha b_\alpha)),$$

$$\frac{\partial n_1}{\partial t} = -\gamma_1 n_1 + \sum_\alpha ((p^*_{1\alpha} a_{1\alpha} + p_{1\alpha} a^*_{1\alpha}) + (q_\alpha b^*_\alpha + q^*_\alpha b_\alpha)),$$

$$\frac{\partial p_{2\alpha}}{\partial t} + (\alpha_2 - i\Delta_2) p_{2\alpha} = (n_3 - n_2) a_{2\alpha} - q^*_\alpha a_{1\alpha} - p_{1\alpha} b^*_\alpha,$$

$$\frac{\partial p_{1\alpha}}{\partial t} + (\alpha_1 - i\Delta_1) p_{1\alpha} = (n_3 - n_1) a_{1\alpha} - q_\alpha a_{2\alpha} + p_{2\alpha} b_\alpha,$$

$$\frac{\partial q_\alpha}{\partial t} + (\alpha_3 - i(\Delta_1 - \Delta_2)) q_\alpha = p_{1\alpha} a^*_{2\alpha} + p^*_{2\alpha} a_{1\alpha} + (n_2 - n_1) b_\alpha,$$

$$\frac{\partial a_{n\alpha}}{\partial t} - (-1)^\alpha \frac{\partial a_{n\alpha}}{\partial x} = \beta_n p_{n\alpha} + p_{0n}, \qquad (1)$$

where $a_{n\alpha}$ are the amplitudes of the electromagnetic wave in the transitions $3 \leftrightarrow n$; the $p_{n\alpha}$ are the amplitudes of the polarization waves associated with the fields $a_{n\alpha}$. The index α numerates the waves propagating along ($\alpha = 1$) and against ($\alpha = 2$) the x-axis. Eqs. (1) are dimensionless: $x = x'/L$, $t = t'/\tau$, where $\tau = L/c$, and L is the active medium length, therefore $\alpha_n = \tau/T_2^{(n)}$ and $\Delta_n = \tau\Delta\omega_n$ are the dimensionless relaxation rate and detuning. The dimensionless parameters β_n are

$$\beta_1 = \frac{2\pi\omega_{31}|d_{31}|^2}{\hbar}\frac{N}{V}\tau^2,$$

$$\beta_2 = \frac{2\pi\omega_{32}|d_{32}|^2}{\hbar}\frac{N}{V}\tau^2. \qquad (2)$$

We have introduced the spontaneous polarization terms p_{0n} into the right-hand side of the field equations in Eq. (1) to instigate the semiclassical numerical calculation. It should be noted that reasonable variations in the value of p_{0n} do not strongly affect the results.

To describe the situation realized in experiments [1] we should use the following initial and boundary conditions. We assume that all molecules are initially in the ground state and amplitudes of the waves inside the active volume are equal to zero:

$$a_{n\alpha}(x, 0) = 0, \quad p_{n\alpha}(x, 0) = 0, \quad n_{3,2}(x, 0) = 0, \quad n_1(x, 0) = n_0.$$

The pumping pulse enters the active volume from the left side therefore the boundary conditions are

$$a_{11}(0, t) = A(t), \quad a_{21}(0, t) = 0, \quad a_{12}(1, t) = 0, \quad a_{22}(1, t) = 0, \qquad (3)$$

where $A(t)$ is the profile of the pumping pulse, the coordinate $x = 1$ corresponds to the right boundary of the active volume.

3. Long pumping pulse

In the experiments [1] long $\tau_P = 40$ ns and short $\tau_P = 40$ ps pumping pulses have been used. The active medium transit time is about 10 ns, therefore in the first case the dimensionless duration of pumping is about unity, and in the second case it is about 10^{-2}–10^{-3}. Let us start from the first case. For

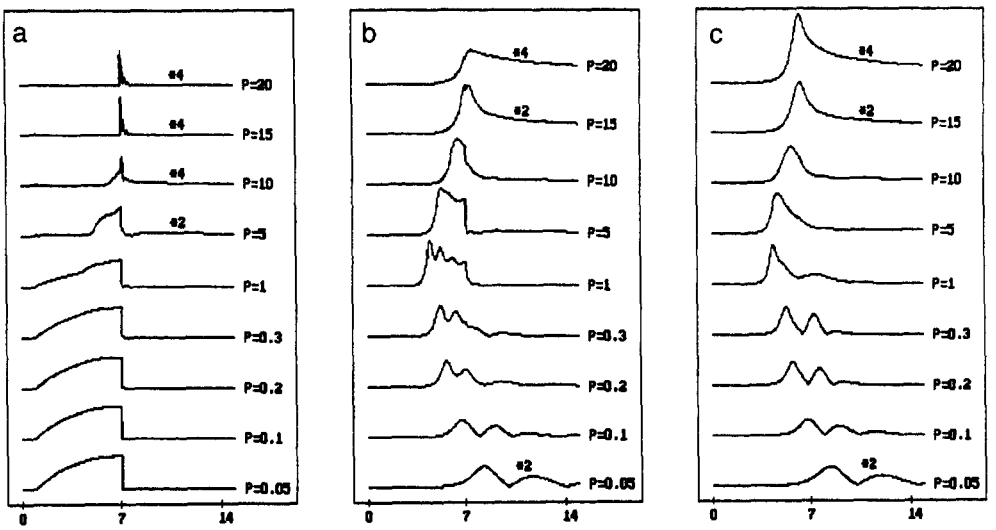

Fig. 1. Intensity profiles for pumping (a), and copropagating (b) pulses at the exit plane of the active medium ($x = 1$), and counterpropagating pulse (c) at the entrance plane ($x = 0$) for different values of the dimensionless pressure. The active medium parameters are $\beta_1 = 0.2$; $\alpha_1 = 4$; $\beta_2 = 17.5p$; $\alpha_2 = 1.46p$. The pumping pulse parameters are $A_0 = 0.73$, $\Delta = 2$.

experiments with CH_3F gas, the dimensionless parameters β_n and α_n can be estimated as follows

$$\beta_2 = 17.5p, \quad \alpha_2 = 1.46p, \quad \beta_1 = 0.2p,$$
$$\alpha_1 \approx 4, \quad \Delta = 2. \qquad (4)$$

The coefficients β_n are proportional to the density of molecules, therefore we assume the linear dependency of β_n on the dimensionless gas pressure p. We may also assume that the collisional relaxation rate is proportional to the gas pressure. The profile of

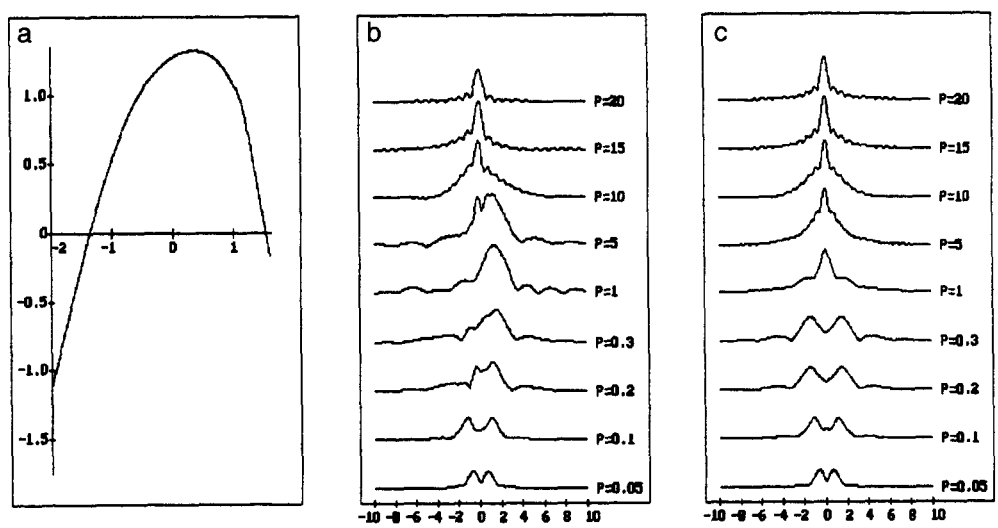

Fig. 2. (a) Peak pulse intensity as a function of pressure in the double logarithmic scale ($\log(I_m)$ vs. $\log(p)$); (b) Power spectrum for forward pulse $I_f = |a_{21}(1,\omega)|^2$; (c) Power spectrum for backward pulse $I_b = |a_{22}(0,\omega)|^2$. The parameters of the medium and pumping pulse are the same as for Fig. 1.

the incident pumping pulse in accordance with [1] is taken in the form

$$A(t) = A_0\left(1 + \frac{t - t_0}{T_1}\right)\exp\left(-\frac{t - t_0}{T_1}\right),$$
$$= A_0\exp\left(-\frac{(t - t_0)}{T_2}\right) \quad (5)$$

where t_0 is a delay time, and $T_2 \ll T_1 \approx 1$. The initial population density n_0 (see Eq. (1)) is $n_0 = 20$.

Fig. 1 shows the results of numerical calculations for the intensity profiles for the pumping (Fig. 1a), and copropagating (Fig. 1b) and counterpropagating (Fig. 1c) SR pulses. At low pressure $p < 0.3$ the pumping pulse passes through the gas tube without essential change in its form and intensity. In the region $0.3 < p < 3$ the pumping is more effective, and the intensity of the transmitted pumping pulse decreases. At high pressure $p > 3$, the pumping pulse loses almost all its energy. The profiles of copropagating and counterpropagating SR pulses are similar at low pressure and they became different with the pressure increase. As we can see from Fig. 1b in the region $1 < p < 10$ the copropagating SR pulse has a strong abrupt end at the tail of the pumping pulse, while the counterpropagating pulse has a smooth envelope.

The peak pulse intensities for copropagating and counterpropagating waves as functions of pressure are shown in Fig. 2a in double logarithmic scale. The peak pulse intensities coincide for both waves, while the intensity profiles are different. At the pressure $p < 0.3$, we have the quadratic dependence of intensity versus pressure $I \sim p^2$, which corresponds to superradiance, then intensity saturates and decreases at high pressure. As we have mentioned the carrier frequency of the pumping pulse was detuned from the exact resonance with the transition $3 \leftrightarrow 1$. Therefore the Fourier-transform of the pulse amplitude

$$a(x,\omega) = \int_{-\infty}^{+\infty} a(x,t)\exp(i\omega t)\mathrm{d}t$$

should be shifted from the frequency of transition $3 \leftrightarrow 2$ in the case of stimulated Raman scattering, and the Fourier-transform should be unshifted in the case of superradiance. In Figs. 2b,c, the power spectrum for forward $I_f = |a_{21}(1,\omega)|^2$ and backward $I_b = |a_{22}(0,\omega)|^2$ pulses is shown for different pressure. We can see that for the forward pulse the power spectrum is shifted from the frequency ω_{32} for the pressure in the range $0.2 < p < 10$. The value of the shift approaches the value of pumping pulse detuning $\Delta = 2$. For the backward pulse, the power spectrum is unshifted for any pressure. Comparing Fig. 1b and Fig. 2b, we can see that the process of the stimulated Raman scattering occurs when the pumping pulse and copropagating pulse in the transition $3 \leftrightarrow 2$ overlap. In experiments [1] and in our computer simulations, the area of the pumping pulse is smaller than π for the transition $3 \leftrightarrow 1$. Therefore, the population inversion density in this transition is always negative. Thus, the backward wave in the transition $3 \leftrightarrow 1$ can not be generated, which results in the absence of the SRS process in the transition $3 \leftrightarrow 2$ for the backward wave. For the pumping pulse of high intensity, we can have the SRS both for forward and backward pulses.

Up to now, we have assumed that the pumping pulse was of moderate intensity approximately appropriate to that in experiments [1]. In this case, the threshold conditions for Raman scattering are met at high pressure when the dimensionless relaxation rate α_2 is higher than unity. The condition $\alpha_2 > 1$ means that the relaxation rate T_2 is smaller than the active medium transit time $\tau = L/c$. In this case the SRS process may occur. By increasing the pumping pulse intensity we can realize the conditions for Raman scattering at low pressure, when $\alpha_2 < 1$. In the latter case the conditions for cooperative Raman scattering can be realized.

In Fig. 3, the results of computer simulations are shown for the medium with the parameters $\beta_2 = 1.0p$, $\alpha_2 = 0.01p$ (cf. Eq. (4)) and the pumping pulse amplitude A_0 is seven times higher than that in Fig. 1. Figs. 3a,b show the intensity profiles for forward and backward pulses respectively. The power spectra of these pulses are shown in Figs. 3c,d. The power spectrum of the backward pulse is again unshifted, at the same time the power spectrum for forward pulse has a negative shift for $1 < p < 4$ and a positive shift for $p > 4$. The detuning of the pumping pulse is $\Delta = 2$. For the pressure $1 < p < 4$, the cooperative Raman scattering (CRS) occurs. The shift of the Raman emission is due to the interference of polarizations in the pumping transition $3 \leftrightarrow 1$ and forbidden transition $2 \leftrightarrow 1$. When the pumping pulse is detuned from the resonance with transition

$3 \leftrightarrow 1$, the populations in the third and second levels are modulated at the difference frequency Δ, as a result the polarization wave in the transition $m \leftrightarrow n$ is a triplet with the frequencies ω_{mn} and $\omega_{mn} \pm \Delta$. The amplitudes of these components are determined by the interference conditions. Fig. 3c clearly demonstrates that for the CRS process the highest amplitude has a component of polarization in the transition $3 \leftrightarrow 2$ with the shift opposite to the shift of the pumping pulse, while for SRS process the shift of polarization wave coincides with the shift of the pumping wave. This is a very important difference between the CRS and SRS processes.

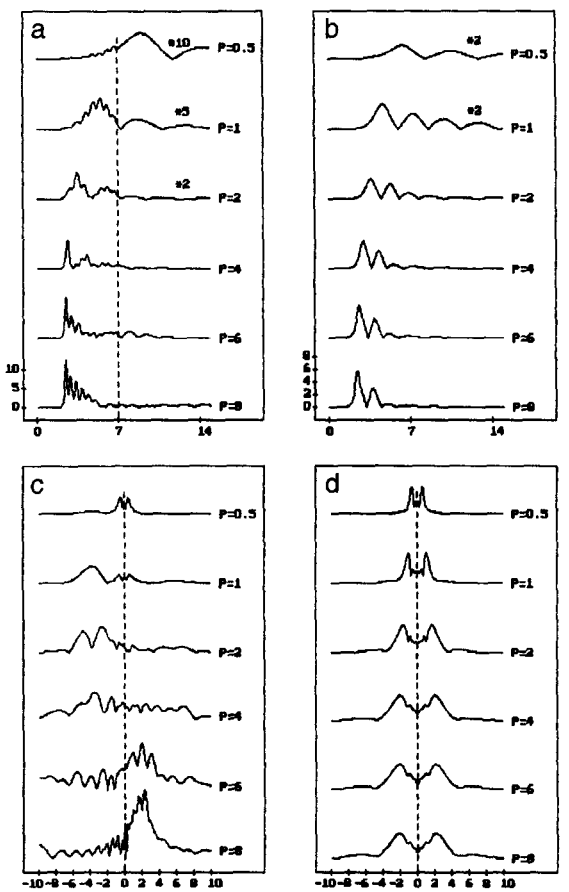

Fig. 3. Intensity profiles for copropagating (a) and counterpropagating (b) pulses for different pressure of molecular gas. Power spectra for copropagating (c) and counterpropagating (d) pulses for different pressure of molecular gas. The vertical dashed line in (a) indicates the tail of the pumping pulse. The active medium parameters are $\beta_1 = 0.05p$; $\alpha_1 = 4$; $\beta_2 = p$; $\alpha_2 = 0.01p$. The pumping pulse parameters are $A_0 = 5.1$, $\Delta = 2$.

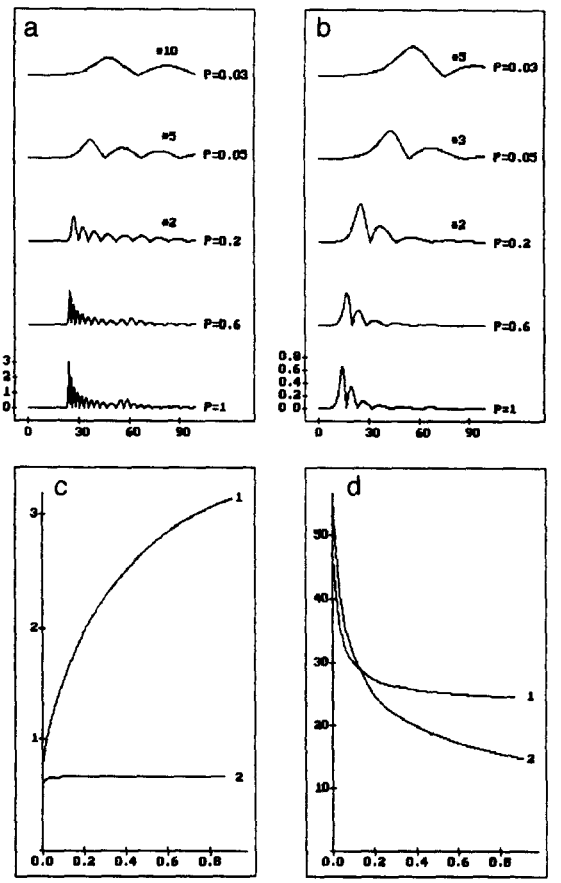

Fig. 4. Intensity profiles for FIR copropagating (a) and counterpropagating (b) pulses for different values of pressure of molecular gas. (c) Peak pulse intensity normalized to pressure for FIR copropagating (curve 1) and counterpropagating (curve 2) pulses as a function of dimensionless pressure. (d) Delay time for FIR copropagating (curve 1) and counterpropagating (curve 2) pulses as a function of dimensionless pressure.

4. Ultrashort pumping pulse

In this Section we discuss the specific features of SR and SRS emission when the picosecond pulse of CO_2-laser is used for pumping. We assume that the pumping pulse has a hyperbolic secant form

$$a_1(t,0) = \frac{S}{\pi\tau_0}\left[\mathrm{ch}\left(\frac{t-t_0}{\tau_0}\right)\right]^{-1},$$

where S is an area of the pumping pulse. In Figs. 4a,b the profiles of SR copropagating and counterpropagating pulses are shown for different pressure of molecular gas. We can see that for lower pressure the delay time for backward emission is longer than for forward emission, while for the high pressure the delay time for backward emission becomes smaller than for forward emission (Fig. 4d). At high pressure the intensity of the forward pulse is significantly higher than the intensity of backward emission and the dynamics of the process is determined primarily by the interaction of pumping and copropagating pulses. The temporal width of the copropagating pulse approaches the pumping pulse width. The ratio of intensities of copropagating and counterpropagating pulses increases with the rise of the active medium length (Fig. 4c).

In Fig. 4c, we can see an interesting feature of the intensity versus pressure dependence for the backward pulse. The intensity of the backward pulse normalized to the gas pressure does not depend on the pressure in the region $p > 0.1$. Hence, when the coherence length is smaller than the active medium length the backward pulse is developed primarily in the coherence volume near the left boundary of the active medium.

Fig. 5 shows the delay time of the copropagating pulse as a function of the active medium length for different values of gas pressure. We can see that at long distances the pumping and forward pulses begin to overlap. When these pulses are overlapping the superradiative emission is substituted by the stimulated Raman scattering emission. The carrier frequency of the forward pulse is shifted if the pumping pulse is detuned from the resonance with the transition $3 \leftrightarrow 1$. The SRS process is accompanied by the appearance of polarization in the forbidden transition $2 \leftrightarrow 1$. We can see such behaviour in Figs. 6a,b where the intensity profile of the forward pulse (Fig. 6a) and polarization q (Fig. 6b) in the transition $2 \leftrightarrow 1$ are shown for different pressures. The dashed vertical line indicates the position of the pumping pulse. It is seen that the polarization q increases significantly with the pressure growth which is followed by the increase of overlapping of pumping and SR pulses. The effect upon the forward pulse

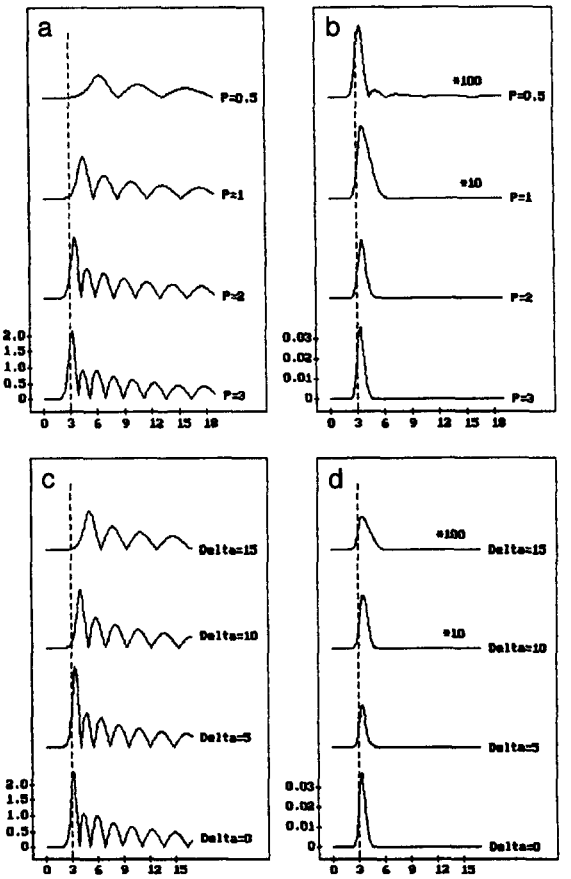

Fig. 6. Intensity profiles of FIR copropagating pulse (a,c) and polarization in the forbidden transition $2 \leftrightarrow 1$ (b,d) for different values of molecular gas pressure (a,b) and detuning of the pumping pulse frequency (c,d) with the resonant frequency in transition $3 \leftrightarrow 1$. The vertical dashed lines indicate the position of the pumping pulse peak.

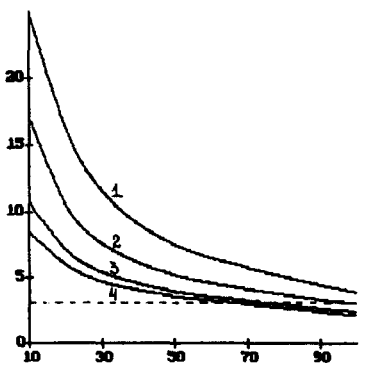

Fig. 5. Delay time as a function of active medium length for different pressure. The dimensionless pressure is $p = 0.5$ (curve 1), $p = 1$ (curve 2), $p = 2$ (curve 3), $p = 3$ (curve 4).

and polarization q profiles in the detuning of the pumping pulse is shown in Figs. 6c,d. We can see that with increasing detuning the delay time increases and polarization in the forbidden transition decreases.

5. Conclusions

The results presented here clearly demonstrate the deterministic effects on SR pulse evolution of the pumping pulse area and detuning, as well as gas pressure. By varying these parameters we can control the intensity, temporal width and carrier frequency of the pulse of the forward emission.

The results of computer stimulations show the significant difference in the process of stimulated and cooperative Raman scattering. In the process of SRS emission the carrier frequency of the pulse is followed by the frequency of pumping. The decrease of the pumping pulse frequency results in the decrease of the SRS pulse frequency. For the CRS process, the decrease of the pumping pulse frequency may result in the increase of the CRS pulse frequency. This feature of CRS emission may be useful for practical applications.

References

[1] D.P. Scherrer and F.K. Kneubühl, Infrared Phys. Technol. 34 (1993) 227.
[2] D.P. Scherrer, A.W. Kälin, R. Kesselring and F.K. Kneubühl, Appl. Phys. B53 (1991) 250.
[3] D.P. Scherrer, A.W. Kälin, R. Kesselring and F.K. Kneubühl, Opt. Comm. 87 (1992) 249.
[4] D.P. Scherrer, J. Knittel, D.B. Moix, M.O. Baumgartner and F.K. Kneubühl, Infrared Phys. Technol. 36 (1995) 395.